Mechanisms, Pathways, and Dynamics of Excited-State Energy Flow in Self-Assembled Wheel-and-Spoke Light-Harvesting Architectures

Hee-eun Song,[†] Christine Kirmaier,[†] Jennifer K. Schwartz,[†] Eve Hindin,[†] Lianhe Yu,[‡] David F. Bocian,[§] Jonathan S. Lindsey,[‡] and Dewey Holten*,[†]

Department of Chemistry, Washington University, St. Louis, Missouri 63130-4889, Department of Chemistry, North Carolina State University, Raleigh, North Carolina 27695-8204, and Department of Chemistry, University of California at Riverside, Riverside, California 92521-0403

Received: June 26, 2006; In Final Form: July 25, 2006

Static and time-resolved optical measurements are reported for two cyclic hexameric porphyrin arrays and their self-assembled complexes with guest chromophores. The hexameric hosts contain zinc porphyrins and 0 or 3 free base (Fb) porphyrins (denoted Zn_6 or Zn_3Fb_3, respectively). The guests are a tripyridyl arene (TP) and a dipyridyl-substituted free base porphyrin (DPFb), each of which coordinates to zinc porphyrins of a host via pyridyl−zinc dative bonding. Each architecture is designed to have an overall gradient of excited-state energies that affords excitation funneling within the host and ultimately to the guest. Collectively, the studies delineate the various pathways, mechanisms, and rate constants of energy flow among the weakly coupled constituents of the host−guest complexes. The pathways include downhill unidirectional energy transfer between adjacent chromophores, bidirectional energy migration between identical chromophores, and energy transfer between nonadjacent chromophores. The energy transfer to the lowest-energy chromophore(s) within the backbone of a hexameric host (Fb porphyrins in Zn_3Fb_3 or pyridyl-coordinated zinc porphyrins in Zn_6·TP and Zn_6·DPFb) proceeds primarily via a through-bond mechanism; the transfer is rapid (∼40 ps depending on the array) and essentially quantitative (≥98%). The energy transfer from a pyridyl-coordinated zinc porphyrin of the host to the Fb porphyrin guest in the Zn_6·DPFb complex is almost exclusively Förster through-space in nature; this process is much slower (∼1 ns) and has a lower yield (65%). These studies highlight the utility of cyclic architectures for efficient light harvesting and energy transfer to a designated trapping site.

I. Introduction

Understanding how to design and construct light-harvesting architectures that absorb light and funnel the resulting energy to a designated site remains a central objective in artificial photosynthesis. The inspiration for the design of synthetic light-harvesting systems stems from the natural photosynthetic systems, where the chlorophyll pigments in the antenna complexes can number in the hundreds. Synthetic light-harvesting arrays generally differ from most natural systems in (1) having fewer numbers of pigments, (2) using porphyrins as surrogates for chlorophylls, and (3) employing covalent linkages between the porphyrins for organization rather than noncovalent interactions in a protein matrix. The synthesis and properties of such multiporphyrin arrays have been extensively reviewed.[1−11] Porphyrinic compounds also have been prepared that undergo self-assembly.[12−18] The synthetic light-harvesting architectures prepared to date are less sophisticated structurally and exhibit poorer performance than natural systems owing both to inadequate synthetic methodology and a lack of knowledge concerning how to design efficient light-harvesting systems. Accordingly, versatile molecular architectures that provide insight into how to control the flow of energy remain of great importance.

Several years ago we reported the synthesis of cyclic hexameric arrays of porphyrins for studies of light-harvesting phenomena (Chart 1).[19−21] The chief motivation for preparing cyclic arrays originated with the finding that the light-harvesting antenna complexes of photosynthetic bacteria are organized in large cyclic assemblies. Added impetus stemmed from the possibility of exploiting the three-dimensional architecture of cyclic arrays for host−guest and energy-funneling studies. In this regard, energy-transfer modeling studies have indicated that cyclic architectures are intrinsically more efficient than linear or dendrimeric architectures in funneling energy to a single trapping site.[22] The synthesis of the cyclic hexamers shown in Chart 1 was facilitated by the extensive prior work of Anderson and Sanders, who described the synthesis and host−guest properties of diverse cyclic arrays composed of two, three, or four porphyrins.[23] In the past two years, remarkably large cyclic arrays (containing as many as 24 porphyrins) have been constructed.[24−30] However, to date only a handful of cyclic multiporphyrin arrays has been shown to bind a guest porphyrin, as is desired for energy-funneling studies.[31−34]

Chart 1 shows structures of two cyclic hexameric porphyrins comprised of zinc porphyrins and 0 or 3 free base (Fb) porphyrins (denoted Zn_6 or Zn_3Fb_3, respectively). The porphyrins are linked via diphenylethyne units. The cyclic arrays are reasonably shape-persistent[35] and have a cavity diameter of ∼34 Å. Chart 1 also shows a tripyridyl arene (TP) and a dipyridyl-substituted Fb porphyrin (DPFb), each of which can coordinate in a hexameric array via pyridyl−zinc dative bonding to give a self-assembled host−guest complex. The structures of the self-assembled complex of Zn_6 with the TP guest (denoted Zn_6·TP) and of Zn_6 with the dipyridyl Fb porphyrin (denoted Zn_6·DPFb)

* Author to whom correspondence should be addressed. E-mail: holten@wustl.edu.
[†] Washington University.
[‡] North Carolina State University.
[§] University of California at Riverside.

10.1021/jp064000i CCC: $33.50
Published on Web 09/13/2006

CHART 1

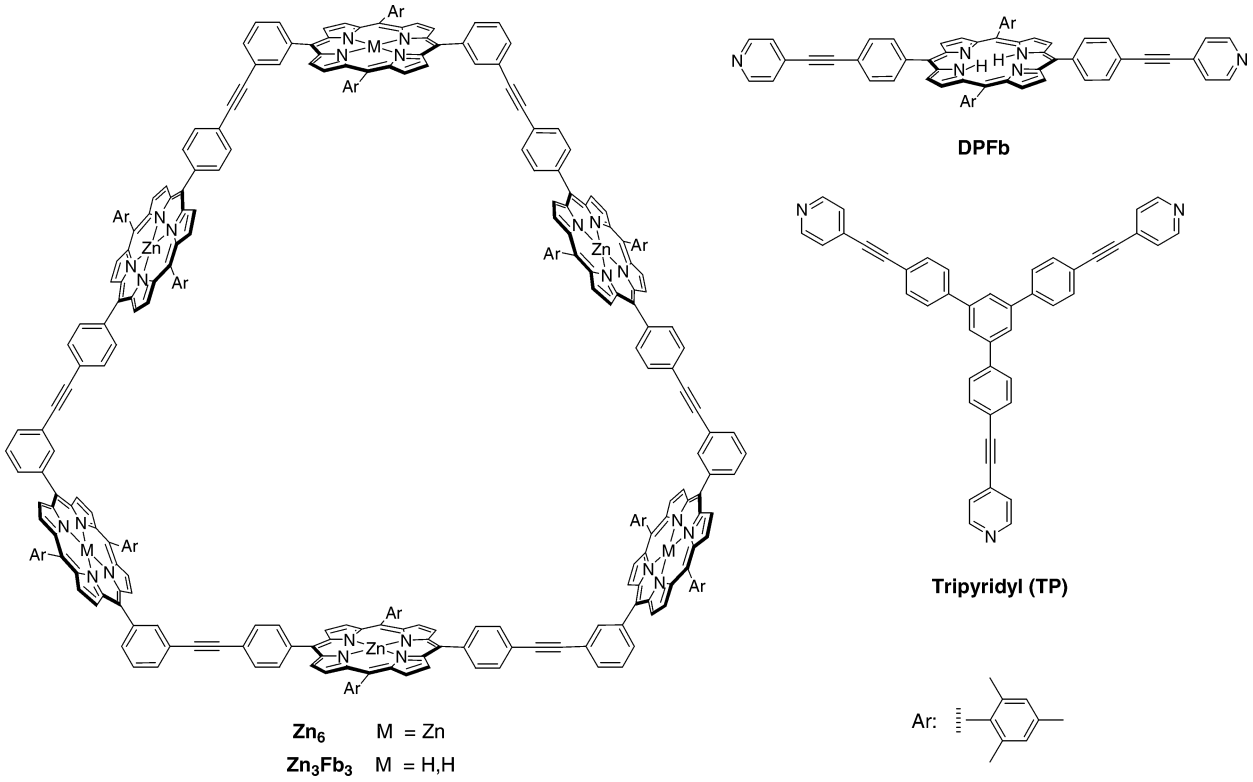

are shown in Chart 2. Both host−guest architectures assemble with very high affinity ($K_{assoc} > 3 \times 10^8$ M^{-1}) in toluene at room temperature and thus are >95% assembled upon mixing the host and guest in 1:1 ratio at 1 μM concentrations.[34]

The cyclic hexameric structure of Zn_3Fb_3 has been confirmed by high-angle X-ray scattering studies in toluene solution.[36] Such analyses showed that (1) the cyclic hexameric architecture is not rigid but is distributed across a conformational ensemble with a mean diameter that is 1.5 Å smaller than the diameter of a symmetric, energy-minimized model structure, (2) the conformational envelope has limits of 3 Å positional dispersion and full rotational freedom for all six porphyrin groups, and (3) insertion of the TP guest to give Zn_3Fb_3·TP expands the diameter of the host conformer by 0.6 Å and decreases the amplitude of the configurational dispersion by ~2-fold. Molecular dynamics simulations for Zn_3Fb_3 show bowing and rotations of all six porphyrin groups, particularly those porphyrins that contain *p*-ethynyl-substituted meso substituents (i.e., the zinc porphyrins in Zn_3Fb_3), while retaining the overall macrocyclic architecture. The extent of conformational motion is restricted in Zn_3Fb_3·TP versus that in Zn_3Fb_3. The guest porphyrin DPFb is expected to undergo rotation about its linear axis in the host Zn_6 owing to the presence of the *p*-ethyne substituents in DPFb and the large cavity of the cyclic hexameric host.

In previous studies of acyclic diarylethyne-linked arrays, we found that the energy-transfer process between porphyrins is predominantly through-bond (TB) rather than Förster through-space (TS) in nature.[37] The majority of our studies concerned unidirectional (downhill) transfer processes between a zinc porphyrin and a Fb porphyrin. We also characterized the rate of reversible energy transfer between identical, isoenergetic zinc porphyrins.[38] A further set of studies characterized the transfer between nonadjacent chromophores.[39]

The cyclic hexameric host−guest complexes provide an opportunity to probe energy flow in small arrays wherein all of the above energy-transfer processes are operative within the backbone of the host, in addition to subsequent transfer to the core guest porphyrin. A key objective is to assess the magnitude of the various processes so as to better understand how to design more efficient light-harvesting architectures. To do so requires an in-depth understanding of the mechanism and rate of each of the processes.

In this paper, we report the characterization of the multiple pathways for excited-state energy flow in cyclic hexameric arrays (Zn_6, Zn_3Fb_3) and the corresponding self-assembled host−guest constructs (Zn_6·TP, Zn_6·DPFb). In the Zn_6 host, all the chromophores are isoenergetic and energy flows between the zinc porphyrins; in the Zn_3Fb_3 host, energy transfer is downhill from the zinc to the Fb porphyrins. In the Zn_6·DPFb host−guest assembly, the lowest-energy chromophores in the backbone of the array are the two zinc−pyridyl-coordinated porphyrins, and the lowest overall energy chromophore is the Fb porphyrin in the guest. The results reported herein show that energy transfer within the backbone of the array is very fast, whereas transfer from a zinc−pyridyl-coordinated porphyrin to the Fb porphyrin guest is surprisingly slow. The companion paper reports the characterization of architecturally more complex arrays composed of distinct patterns of zinc and Fb porphyrins where the lowest-energy chromophore in the backbone of an array is not the pyridyl-coordinated zinc porphyrin but rather a Fb porphyrin.[40] Taken together, these studies provide valuable insight for the design of more efficient self-assembled light-harvesting arrays.

II. Experimental Methods

A. Compounds. The cyclic hexamer hosts (Zn_6 and Zn_3Fb_3),[19] guests (TP[19] and DPFb[34]), reference dyads (ZnFb-*m*/*p*, ZnFb-*p*/*m*, and ZnZn-*m*/*p*),[19] and reference monomers (ZnU and FbU)[41] were prepared as described previously. The self-assembled host−guest complexes (Zn_6·TP and Zn_6·DPFb) were

CHART 2

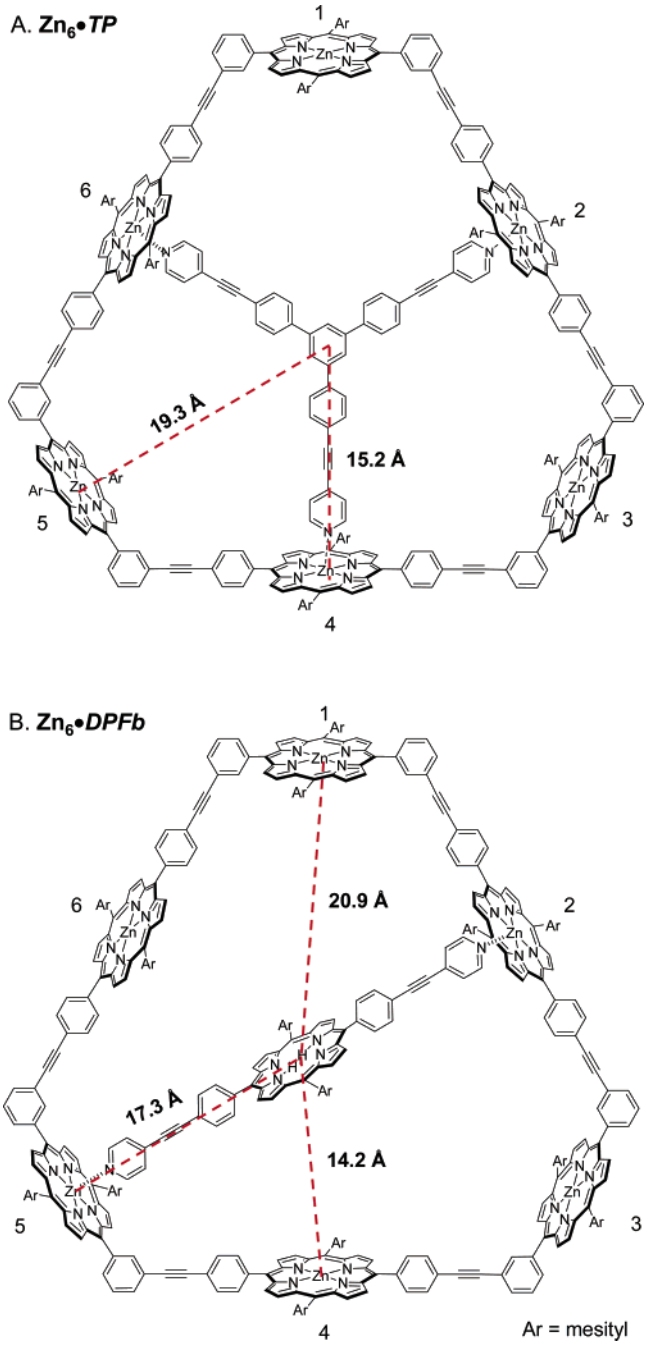

prepared via titrations of stock toluene solutions of the host and guest compounds as described previously[19,34] and in the Supporting Information. All of the above arrays were studied in toluene.

The cyclic hexamers Zn_6•pyr_6 and Zn_3Fb_3•pyr_3, dyad ZnZn•pyr_2, and monomer ZnU•pyr, in which each of the zinc porphyrins is singly coordinated by a pyridine (pyr) ligand, were prepared by adding a ~10^4-fold molar excess of pyridine to a toluene solution of Zn_6, Zn_3Fb_3, ZnZn-*m*/*p*, or ZnU, respectively. The half-ligated hexamer Zn_6•pyr_3 and dyad ZnZn•pyr were similarly prepared using a lower concentration of pyridine. In all cases, the concentration of pyridine was less than 0.1% v/v. (For Zn_6•pyr_3 there will be a random distribution of uncoordinated and coordinated porphyrins.) The arrays Zn_6•pyr_6, Zn_3Fb_3•pyr_3, ZnZn•pyr_2, ZnU•pyr, Zn_6•pyr_3, and ZnZn•pyr were studied in the toluene/pyridine mixture in which they were prepared.

B. Optical Spectroscopy. Static absorption spectra (Cary 100) and fluorescence spectra and quantum yields (Spex Tau2; 5 nm band-pass) employed nitrogen-purged solutions (1−10 μM for absorption and 0.3−1 μM for emission). Fluorescence yields were obtained using nondegassed ZnTPP in toluene (Φ_f = 0.030) as a standard.[42] Fluorescence lifetime studies employed 0.3−3 μM nitrogen-purged solutions. The latter studies used either (1) a phase modulation technique in which emission was collected using a long-pass filter[43] or (2) a single-shot method employing 30 ps, 2 mJ, 532 nm excitation flashes and a detection system with an ~1 ns instrument response function in which emission was collected with a monochromator having a 10 nm band-pass.[44] Transient absorption measurements utilized nondegassed 50−150 μM solutions excited with ~130 fs, ~20 μJ, 530−550 nm excitation flashes and white-light probe pulses of comparable duration.[45] All measurements were carried out at room temperature. Kinetic modeling utilized the program KINSIM[46] as discussed previously.[38]

III. Results and Discussion

A. Molecular Architectures. Chart 3 gives schematic representations of the hexameric arrays (Zn_6, Zn_3Fb_3) and host−guest complexes (Zn_6•TP, Zn_6•DPFb), along with the reference dyads (ZnZn, ZnFb), and reference arrays wherein pyridine (pyr) is coordinated to all of the zinc porphyrins (ZnFb•pyr, ZnZn•pyr_2, Zn_6•pyr_6, Zn_3Fb_3•pyr_3) or one-half of the zinc porphyrins (ZnZn•pyr, Zn_6•pyr_3). The arrows denote the various pathways by which energy transfer can occur. For clarity, only one process of a given type is indicated within each array. Structures of the reference monomers and dyads are given in Chart 4.

The key features of the self-assembled host−guest complexes that are relevant for understanding the energy-transfer dynamics are as follows. A dipyridyl-substituted porphyrin guest is necessarily equidistant (17.3 Å) from the two "bookend" zinc porphyrins to which it is coordinated (porphyrins 2 and 5 in Chart 2B). However, the distances to the guest from the uncoordinated porphyrins in the hexamer differ with position (e.g., porphyrins 1 and 4 in Chart 2B; 20.9 versus 14.2 Å). All distances were established by molecular modeling as described previously.[19] The pyridyl-coordinated zinc porphyrins (denoted Zn_C) have a first excited singlet state at a lower energy than uncoordinated zinc porphyrins (denoted Zn_U) (e.g. Charts 3A and 3B). On the basis of the average (0,0) absorption and fluorescence wavelengths, the excited-state energy decreases in the order: Zn_U (2.08 eV) > Zn_C (2.04 eV) > DPFb (1.91 eV). This energy ordering is a key determinant of the pathways of energy flow in the arrays.

B. Overview of Energy-Transfer Pathways and Mechanisms. An overview of operable energy-transfer processes in the arrays simplifies the presentation of the results. Of all the processes illustrated in Chart 3, the only one for which we have previously measured a rate within a cyclic hexamer is the $Zn_U^*Fb \rightarrow Zn_UFb^*$ energy transfer in Zn_3Fb_3 (Chart 3D).[19] A rate constant $k_1 = (34 \pm 4\ \text{ps})^{-1}$ was obtained, with which the value $(38 \pm 4\ \text{ps})^{-1}$ obtained here agrees well. These values for k_1 in the cyclic hexamer are quite similar to those we previously measured for both the ZnFb-*m*/*p* and ZnFb-*p*/*m* dyads (Charts 3H and 4), for which $k_1 = (40 \pm 4\ \text{ps})^{-1}$.[19] The latter results indicate that the energy-transfer dynamics are the same whether the zinc and Fb porphyrins are attached to the diphenylethyne linker via *m*/*p* or *p*/*m* connectivity. We will assume that the analogous connectivity independence is true for other processes within the cyclic hexamers, as is implicit in

CHART 3

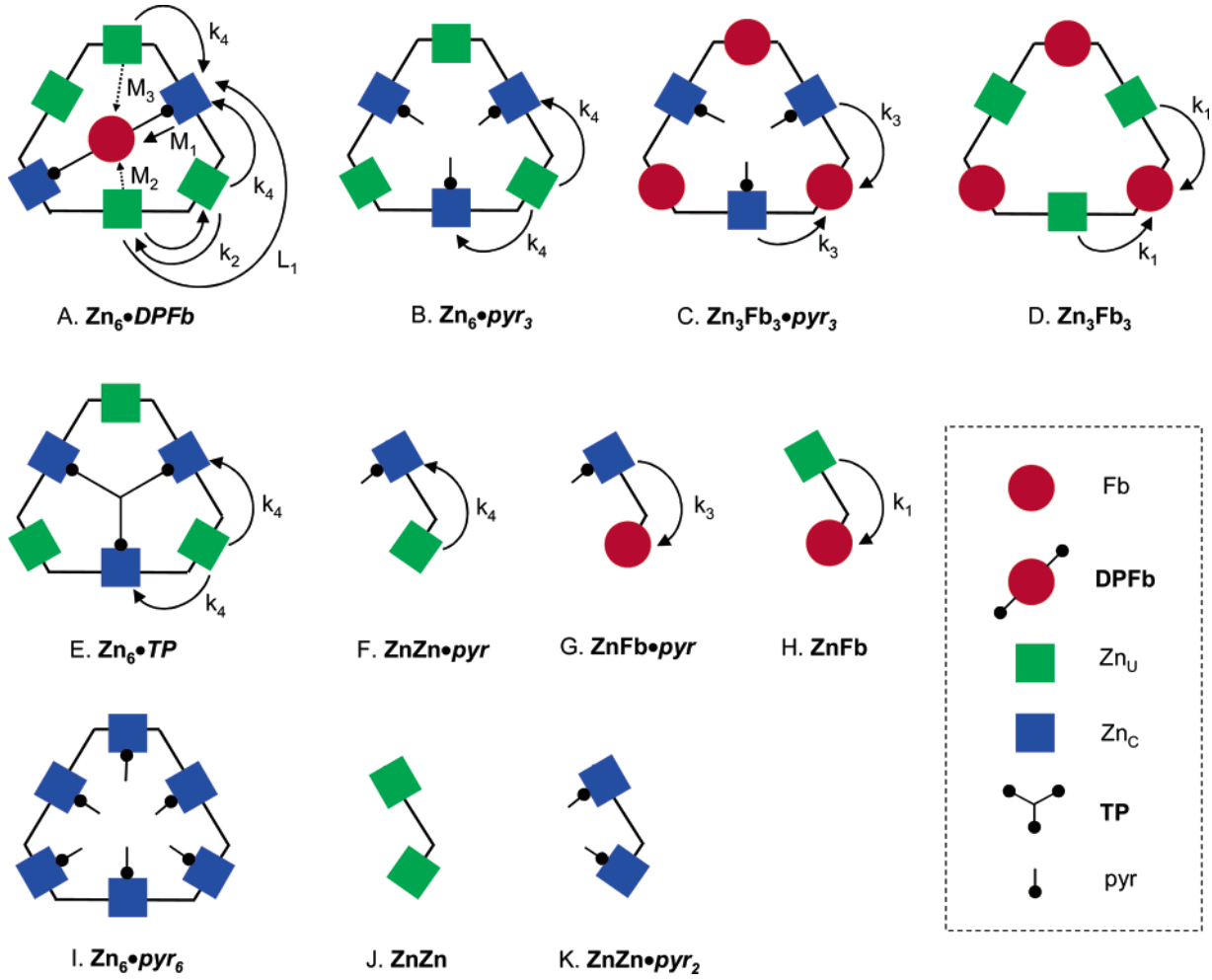

the kinetic schemes shown in Chart 3. This includes $Zn_U^*Zn_C \rightarrow Zn_UZn_C^*$ (k_4; Charts 3A, 3B, and 3E) and $Zn_C^*Fb \rightarrow Zn_CFb^*$ (k_3; Chart 3C). By analogy with our prior studies of energy transfer between diarylethyne-linked porphyrins, all of the above processes within the cyclic hexameric hosts occur predominantly by a linker-mediated TB electron-exchange mechanism, with minimal contribution from the Förster TS mechanism.[37]

In addition to unidirectional energy transfers, bidirectional energy transfer can also occur between adjacent identical zinc porphyrins within the cyclic hexamers, namely, $Zn_U^*Zn_U \leftrightarrows Zn_UZn_U^*$ (k_2; Chart 3A). The rate constant for such a process is typically difficult to obtain owing to the absence of a simple spectral handle to monitor the dynamics. In this regard, we recently studied a large series of linear and branched architectures containing multiple zinc porphyrins and an energy trap.[38,39,47] Kinetic modeling of the measured excited-state dynamics yielded a rate constant of $(30 \pm 10\ \text{ps})^{-1}$ for bidirectional energy transfer between adjacent Zn_U porphyrins joined with diphenylethyne linkers and *p*/*p* connectivity (Chart 5B). This value can be scaled to estimate k_2 for the analogous process involving *m*/*p* connectivity between adjacent Zn_U porphyrins in the cyclic hexamers (Chart 3A). The scaling factor is obtained from the ratio of measured rates of $Zn_U^*Fb \rightarrow Zn_UFb^*$ energy transfer in the dyads ZnFb-*p*/*m* and ZnFb-*p*/*p* (Charts 3H, 4, and 5A), namely, $(40\ \text{ps})^{-1}$ versus $(24\ \text{ps})^{-1}$. Thus, we estimate that $k_2 \approx (30\ \text{ps})^{-1}(24/40) = (50\ \text{ps})^{-1}$ for bidirectional $Zn_U^*Zn_U \leftrightarrows Zn_UZn_U^*$ energy transfer within the cyclic hexamers(Chart 3A). These bidirectional processes are also expected to occur primarily by a linker-mediated TB mechanism.

By analogy to the unidirectional and bidirectional energy transfer steps involving adjacent porphyrins of the hexameric wheels, processes involving nonadjacent porphyrins can also have a significant impact on energy flow. These nonadjacent transfers (L_1 in Chart 3A) occur by a TB superexchange mechanism mediated by the intervening porphyrins (and linkers). Our previous studies of diarylethyne-linked multiporphyrin arrays have shown that unidirectional nonadjacent transfers between first nonnearest neighbors in diarylethyne-linked porphyrins have rate constants that are on the average only 10-fold smaller than the analogous adjacent transfers.[38,39] This point is illustrated in Chart 5B, where the rate of energy transfer from a zinc porphyrin to a nonadjacent Fb porphyrin through an intervening zinc porphyrin in a diphenylethyne-linked triad having *p*/*p* connectivity occurs with a rate constant of $\sim(200\ \text{ps})^{-1}$. Our modeling further indicated that the analogous, bidirectional process involving nonadjacent zinc porphyrins has a rate constant of $\sim(1\ \text{ns})^{-1}$ (Chart 5C). Accordingly, we expect that nonadjacent energy transfers within the hexameric arrays involving the first nonnearest neighbor energetically distinct porphyrins have a rate constant $L_1 \approx (300-600\ \text{ps})^{-1}$. Processes involving the second nonnearest neighbors are expected to be much slower and are ignored.

Despite the underlying kinetic complexity in large multiporphyrin arrays, the measured and modeled time evolution of the

CHART 4

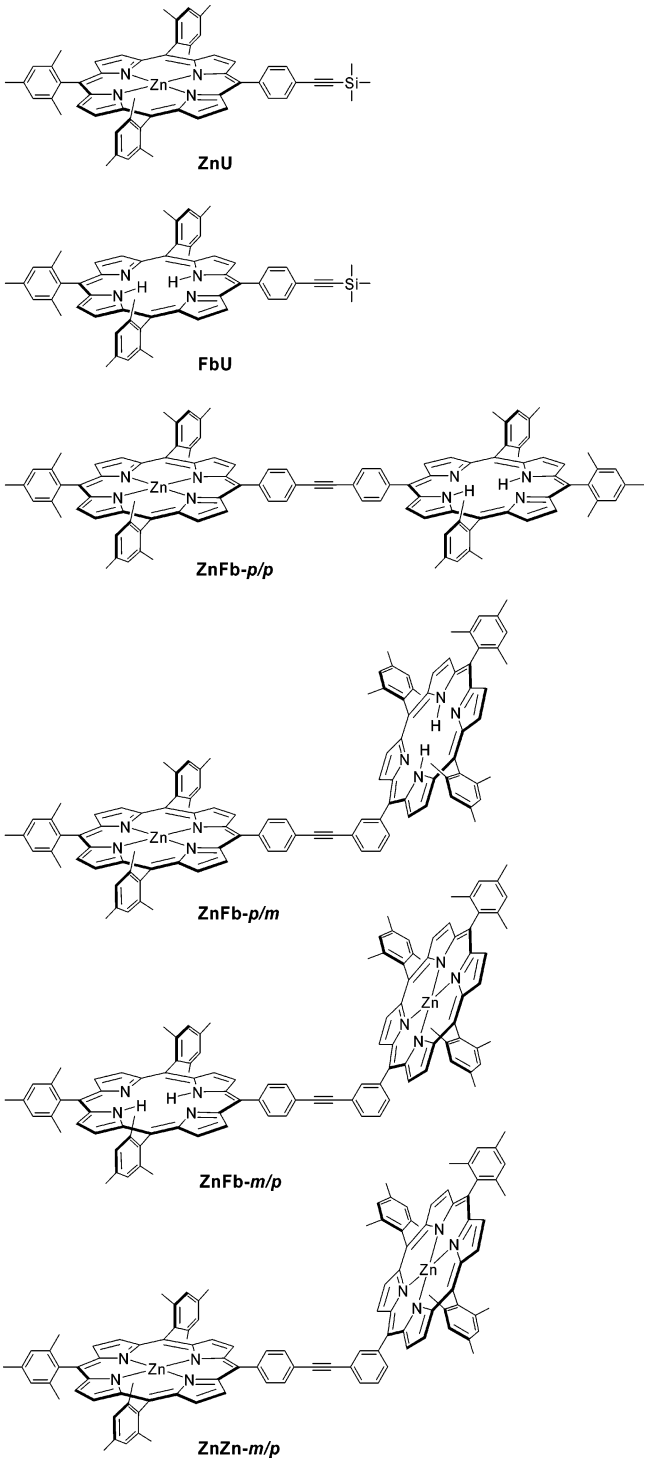

excited-state populations can be fit primarily with a single exponential reflecting the effective rise of energy at the trap site (τ_{rise}) and the lifetime of the composite zinc porphyrin manifold. This is true even for branched architectures containing up to 21 porphyrins in which the distant zinc porphyrins are separated from the trap by two intervening zinc porphyrins using *p*/*p* connectivity.[38] For example, τ_{rise} increases from ~25 to ~50 to ~100 ps along the series in Chart 5.

The pathways and estimated rate constants described above are a starting point for the elucidation of the energy-transfer dynamics among the components of the hexameric wheels. The host−guest complexes contain one or more additional processes underlying the ultimate trapping steps to the DPFb guest

CHART 5

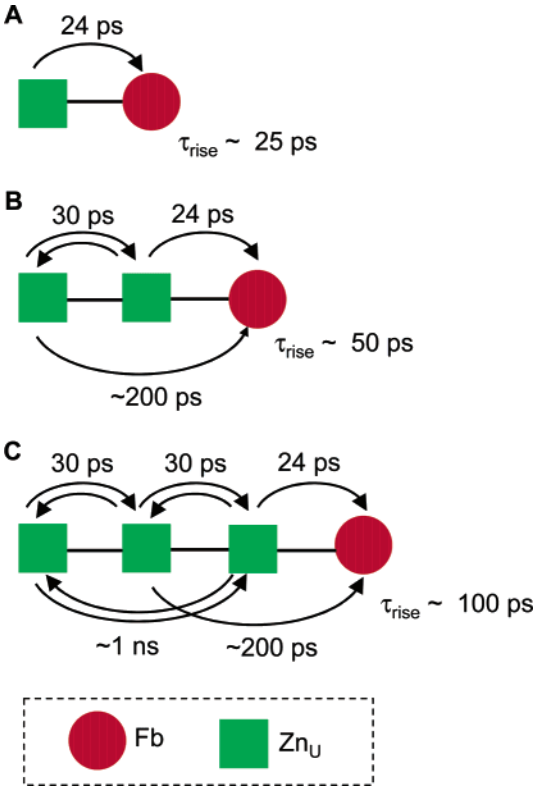

chromophore (M_1−M_3; Chart 3A). The final trapping step is Zn_C^*DPFb → Zn_CDPFb* in Zn_6·DPFb (M_1; Chart 3A) because (1) the "bookend" coordinated zinc porphyrins are the lowest-energy components within the backbone and (2) the TB transfer to these Zn_C units is expected to compete effectively with TS transfer from the Zn_U units to the central trap (M_2 and M_3).

C. Energy Transfer in the Hexameric Hosts. To guide the presentation of the results, Table 1 summarizes the time constants of the kinetic components derived from the transient absorption measurements. The table also contains the associated fluorescence yields and lifetimes, which are dominated by the lowest-energy site(s) in each architecture.

1. Zn_6 and Zn_6·TP. Figure 1B shows absorption and fluorescence spectra of Zn_6. The figure also shows the corresponding spectra of Zn_6 wherein each zinc porphyrin has a pyridine axial ligand, Zn_6·pyr_6. When the zinc porphyrins are uncoordinated, Zn_6 has a split Soret absorption (due to strong exciton coupling) with maxima at 423 and 429 nm, Q(1,0) and Q(0,0) absorption bands at 550 and 590 nm, and Q(0,0) and Q(0,1) fluorescence features at 599 and 646 nm, respectively. For Zn_6·pyr_6, the absorption maxima are red-shifted to 430, 437, 563, and 607 nm, as are the fluorescence bands at 614 and 663 nm.

The fluorescence yield ($\Phi_f = 0.040$) and lifetime ($\tau = 2.4$ ns) of the zinc porphyrins in Zn_6 are similar to those of monomeric reference porphyrins such as ZnU (Chart 4 and Table 1). The fluorescence yield is slightly increased (0.054), and the lifetime is slightly decreased (2.1 ns) in Zn_6·pyr_6. These differences can be traced to an increased $S_1 \rightarrow S_0$ radiative rate constant (k_f) upon ligation based on the values calculated from the formula $k_f = \Phi_f/\tau$ or the integrated intensity of the Q-band absorption manifold.

The absorption and fluorescence spectra of the Zn_6·TP complex (Chart 3E) are shown in Figure 1A and are in good agreement with those reported previously.[34] Comparison of the fluorescence spectrum (Figure 1A), quantum yield, and lifetime (Table 1) with those for Zn_6 and Zn_6·pyr_6 shows that fluores-

TABLE 1: Summary of Photophysical Data[a]

	transient absorption lifetime components (ps)			fluorescence			
					τ (ns)[b]		
compounds	*c*	*d*	*e*	Φ_f	Zn	Fb_{host}	Fb_{guest}
Host−Guest Complexes							
Zn_6·DPFb	3.1 ± 0.7	33 ± 9	730 ± 80	0.084	0.9		11
Zn_6·TP				0.055[f]	2.1		
Hosts							
Zn_6				0.040	2.4		
Zn_6·pyr_6				0.054	2.1		
Zn_3Fb_3		19 ± 2		0.11		13	
Zn_3Fb_3·pyr_3		19 ± 2					
Guest							
DPFb				0.13			13
Reference Compounds							
ZnZn-*m/p*	2.7 ± 0.3			0.040[g]	2.2[g]		
ZnZn·pyr_2	3.6 ± 0.8						
ZnZn·pyr		41 ± 7					
ZnFb-*m/p*		39 ± 4[h]		0.11[g]	0.039[g]	13.5[g]	
FbU				0.12[h]		13.3[h]	
ZnU				0.034[i]	2.4[i]		
ZnU·pyr				0.037	2.2		

[a] All data were obtained at room temperature. Compounds with no pyridine (pyr) ligands on zinc porphyrins were studied in toluene, whereas compounds with one-half or all the zinc porphyrins ligated were studied in toluene plus pyridine. [b] Lifetimes ±7%. [c] Excited-state annihilation. [d] Energy transfer within the hexameric host. [e] Time constant of energy flow from host to guest. [f] The same value for Zn_6·TP (0.055) within experimental error is obtained when taking into account the absorption and fluorescence yields of the uncoordinated and coordinated zinc porphyrins at the excitation wavelength. [g] From ref 19. [h] From ref 50. [i] From ref 51.

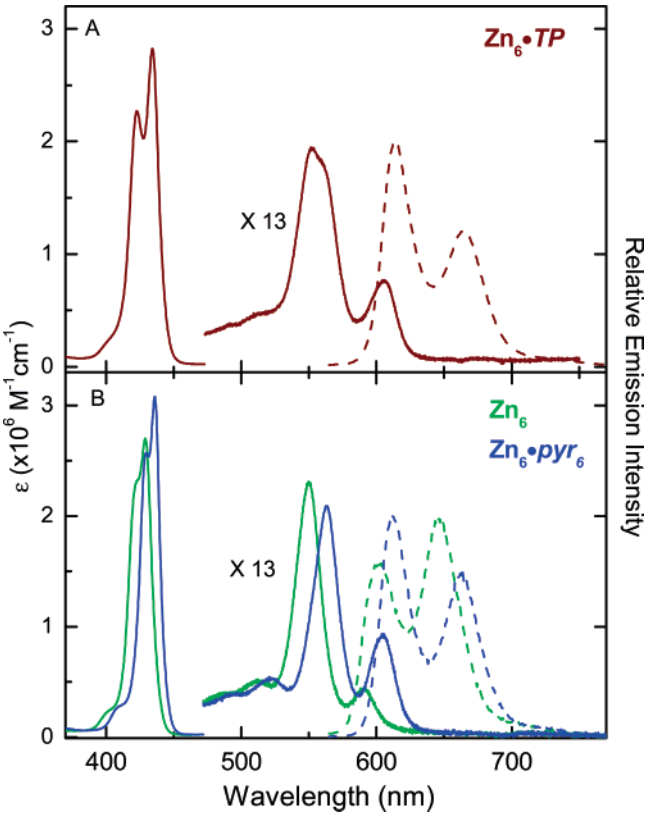

Figure 1. Absorption (solid lines) and fluorescence (dashed lines) spectra of (A) Zn_6·TP (maroon) and (B) Zn_6 (green) and Zn_6·pyr_6 (blue).

cence from the complex occurs almost exclusively from the coordinated zinc porphyrins, even when the uncoordinated components are preferentially (~80%) excited at 550 nm (Figure 1B). In the case of Zn_6·TP, this result is indicative of essentially

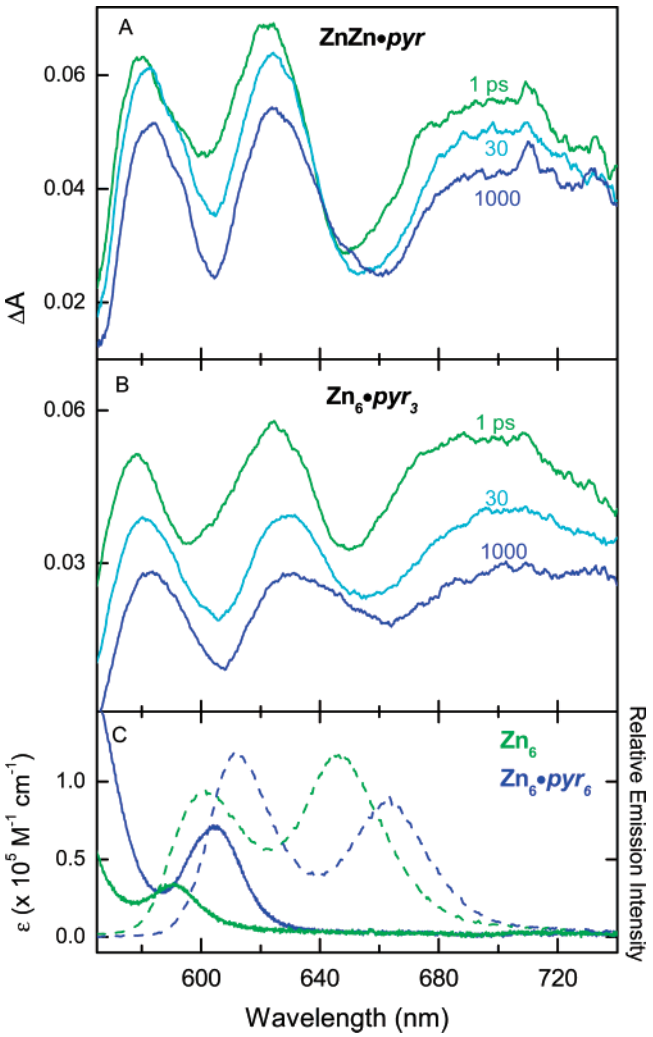

Figure 2. Transient absorption spectra for (A) ZnZn·pyr and (B) cyclic hexamer Zn_6·pyr_3 obtained using a 130 fs excitation flash at 540 nm. Panel C shows the Q(0,0) ground-state absorption band (solid lines) and spontaneous fluorescence spectra (dashed lines) for Zn_6 (green) and Zn_6·pyr_6 (blue).

quantitative $Zn_U^*Zn_C \rightarrow Zn_UZn_C^*$ energy transfer, as has been reported previously.[34]

We had anticipated performing transient absorption experiments on Zn_6·TP to directly measure the rate of this process. However, such measurements were not possible because sufficiently concentrated solutions (~50 μM) could not be obtained. Given that the hexamers themselves are sufficiently soluble, as is the complex containing the dipyridyl-substituted porphyrin guest (Zn_6·DPFb), the low solubility of the TP-containing arrays is presumably due to diminished molecular motion. Thus, we adopted an alternative strategy using coordination with pyridine as described in the next section.

2. Zn_6·pyr_3 and ZnZn·pyr. Solutions of the half-ligated hexamer (Zn_6·pyr_3) and dyad (ZnZn·pyr) were excited with a 130 fs excitation flash at 540 nm, which preferentially (but not exclusively) pumps an uncoordinated zinc porphyrin. Time-resolved absorption difference spectra of these compounds are shown in Figures 2A and 2B. To aid in assignment of the features, Figure 2C shows the Q(0,0) ground-state absorption band (solid lines) and the Q(0,0) and Q(0,1) static spontaneous fluorescence bands (dashed lines) of Zn_6 and Zn_6·pyr_6.

Two main features are present in the absorption difference spectra for both ZnZn·pyr and Zn_6·pyr_3 (Figures 2A and 2B). The spectrum at 1 ps for each array is dominated by features

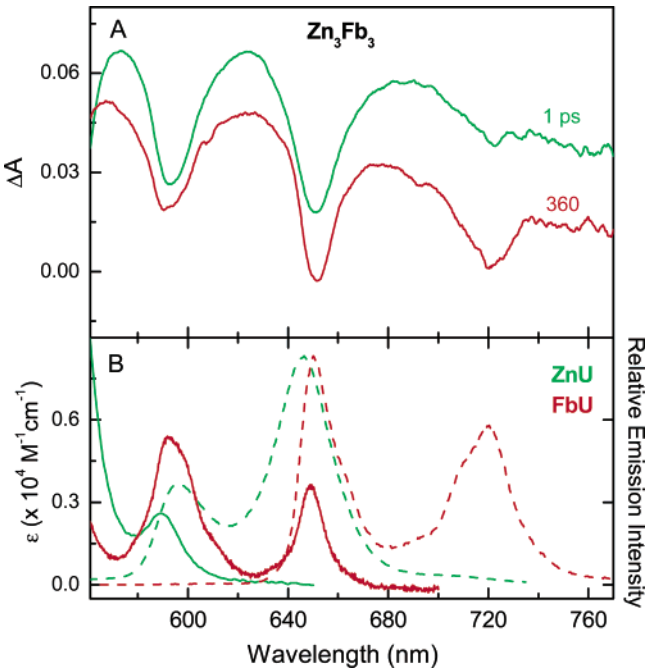

Figure 3. Transient absorption spectra for (A) Zn_3Fb_3 obtained using a 130 fs excitation flash at 540 nm. Panel B shows absorption (solid lines) and fluorescence (dashed lines) spectra of the reference compounds ZnU (green) and FbU (red).

expected for Zn_U^*, which is the component primarily excited by the pump pulse. The feature at ~600 nm contains a contribution of bleaching of the corresponding Q(0,0) ground-state absorption band plus Q(0,0) stimulated emission. This emission is stimulated by the white-light probe pulse and has characteristics (shape and wavelength) similar to those in the analogous spontaneous fluorescence spectrum of Zn_U^* (Figure 2C, green). The absorption difference spectrum at ~1 ns (and much earlier) for both half-ligated arrays exhibits features that are red-shifted from those present at 1 ps. The red shift occurs because the features now correspond to those expected for the formation of Zn_C^* based on the static reference data (Figure 2C, blue). Thus, these observations provide direct time-resolved evidence for the downhill energy transfer $Zn_U^*Zn_C \rightarrow Zn_UZn_C^*$, corroborating the findings from the fluorescence spectrum, lifetime, and yield for Zn_6·TP.

The lifetime of photoexcited Zn_U^* was determined from the time constants obtained from the time evolution of the absorption difference spectra over the range from 550 to 770 nm. The excited-state lifetime obtained is 41 ps for both ZnZn·pyr and Zn_6·pyr_3.[48] This Zn_U^* lifetime is much shorter than the value of 2.4 ns that is observed for complexes in which downhill energy transfer cannot occur, such as the Zn_6 hexamer and the ZnU monomer (Table 1). From these values, the rate constant $k_4 = 1/(41\text{ ps}) - 1/(2.4\text{ ns}) = (42\text{ ps})^{-1}$ and yield $\Phi_{trans} = 1 - (41\text{ ps})/(2.4\text{ ns}) = 0.98$ for $Zn_U^*Zn_C \rightarrow Zn_UZn_C^*$ energy transfer are obtained (Charts 3B and 3F).

3. Zn_3Fb_3 and Zn_3Fb_3·pyr_3. Transient absorption spectra for Zn_3Fb_3 are shown in Figure 3A. The spectra were obtained using excitation at 540 nm, which primarily (but not exclusively) pumps a zinc porphyrin in each array. On the basis of the reference static absorption and fluorescence data shown in Figure 3B, the formation of either Zn_U^* or Fb* will exhibit bleaching and/or stimulated emission at ~590 and ~650 nm, albeit with different relative amplitudes. However, only Fb* will have a feature at ~720 nm, namely, Q(0,1) stimulated emission. On this basis, the 1 ps spectrum is assigned primarily to Zn_U^*, with a contribution of Fb* formed directly upon excitation in a fraction of the arrays. As energy flows from Zn_U^* to Fb to form additional Fb*, the stimulated emission at ~720 nm grows in amplitude, and the shorter-wavelength features evolve as well. Well before 360 ps, the spectrum has attained a constant shape that can be assigned to Fb*.

The absorption difference spectra give a Zn_U^* lifetime of 19 ± 2 ps for Zn_3Fb_3. This value is the same within experimental error as the lifetime of 17 ± 2 ps that we obtained previously[19] and is much shorter than the lifetime of 2.4 ns for Zn_U^* in the absence of energy transfer (Table 1). From these data, the rate constant and yield of $Zn_U^*Fb \rightarrow Zn_UFb^*$ transfer are $k_1 = [1/(19\text{ ps}) - 1/(2.4\text{ ns})]/2 = (38\text{ ps})^{-1}$ and $\Phi_{trans} = 1 - [2(19\text{ ps})]/(2.4\text{ ns}) = 0.98$ (Chart 3D). The factor of 2 appears in the calculations because each Zn_U^* has two adjacent Fb porphyrins to which energy transfer may occur. The value of k_1 is the same within error as that of $(40\text{ ps})^{-1}$ for the ZnFb dyads (Chart 3H).[19] Also, upon arrival on the Fb porphyrin, the excited state decays with a (fluorescence) lifetime of ~13 ns that is essentially the same as the value obtained in monomeric reference porphyrins such as FbU (Table 1). This indicates that Fb* in the cyclic hexamer is not affected appreciably by potential competing processes such as charge transfer.

The results obtained for Zn_3Fb_3·pyr_3 (Chart 3C) are similar to those reported above for Zn_3Fb_3 (with the exception of spectral shifts). In particular, the Zn_C^* lifetime in Zn_3Fb_3·pyr_3 is 19 ± 2 ps. Through the use of the Zn_C^* lifetime of 2.1 ns in the absence of energy transfer (Table 1), the rate constant and yield of $Zn_C^*Fb \rightarrow Zn_CFb^*$ energy transfer in Zn_3Fb_3·pyr_3 are calculated to be $k_3 \approx (38\text{ ps})^{-1}$ and $\Phi_{trans} = 0.98$.

Collectively, the above findings on the rates and yields of energy transfer to the lowest-energy component(s) in the hexameric wheels are essential for understanding the dynamics in the host−guest complexes described next and in the companion paper.[40] These values will be used in the analysis of energy flow in the latter arrays, which exhibit the same processes within the host plus one or more additional pathways for energy trapping by the guest chromophore.

D. Energy Transfer in the Zn_6·DPFb Host−Guest Complex. Figure 4 compares the absorption and fluorescence spectra of the Zn_6 host, DPFb guest, and the Zn_6·DPFb complex. The fluorescence feature at 610 nm in Zn_6·DPFb is exclusively the Q(0,0) band of the zinc porphyrins of the host while the feature at 718 nm is exclusively the Q(0,1) band of the guest; the feature at 652 nm derives from both components. On the basis of these spectra, and the measured fluorescence yields of the components, and the fact that the host absorbs 92% of the light at the 550 nm excitation wavelength, the yield of energy transfer from the host to the guest was found to be 0.63. This value is somewhat greater than the yield of 0.4 estimated previously from the emission spectral data.[34]

Fluorescence lifetimes give a second measure of the host-to-guest energy-transfer yield. The fluorescence of Zn_6·DPFb has two lifetime components, with time constants of 0.9 and 11 ns (Table 1). The longer value is only slightly shorter than that for DPFb alone, indicating that the decay of the excited energy trap is not appreciably affected by its presence in the complex. We assign the shorter component to the lifetime of the Zn_C porphyrins in the host (Chart 3A), which is shorter than the lifetime of 2.1 ns found for coordinated Zn_6·pyr_6. These data afford a yield $\Phi_{trans} = 1 - (0.9/2.1) = 0.57$ for Zn_C^*DPFb $\rightarrow Zn_C$DPFb* energy transfer in the Zn_6·DPFb complex.

Time-resolved absorption data give another measure of energy flow within Zn_6·DPFb (Figure 5A). On the basis of the static

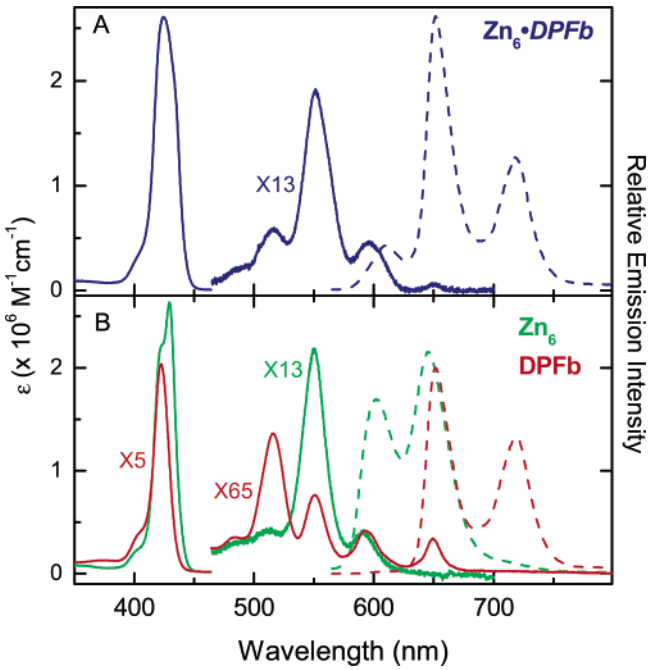

Figure 4. Absorption (solid lines) and fluorescence (dashed lines) spectra of (A) Zn_6·DPFb (navy) and (B) Zn_6 (green) and DPFb (red).

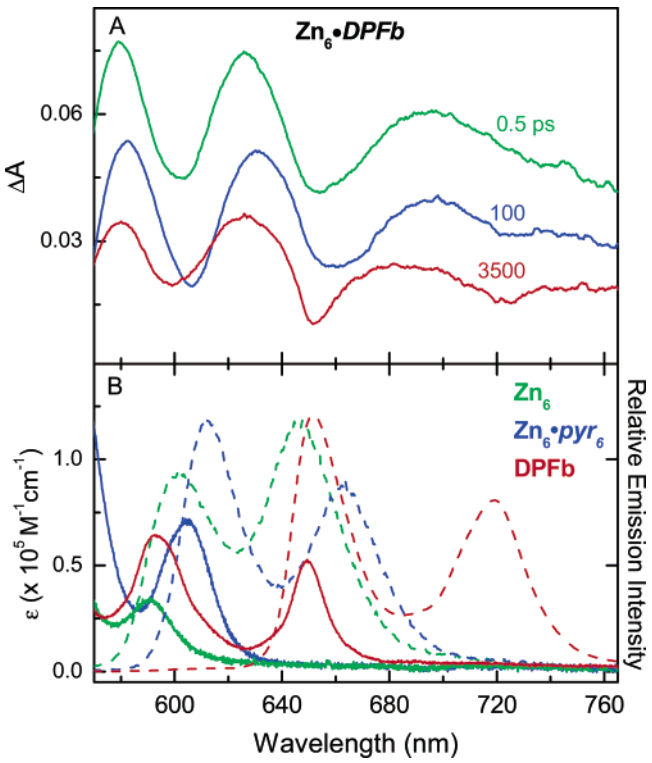

Figure 5. Transient absorption spectra for (A) Zn_6·DPFb obtained using a 130 fs excitation flash at 532 nm. Panel B shows absorption (solid lines) and fluorescence (dashed lines) spectra of Zn_6 (green), Zn_6·pyr_6 (blue), and DPFb (red). Note that the amplitude of the spectrum of DPFb has been magnified 10-fold.

optical data shown in Figure 5B, the 0.5 ps transient difference spectrum contains ground-state bleaching and stimulated emission features associated primarily with Zn_U^* along with a contribution of Zn_C^* produced directly by the 532 nm excitation flash in a fraction of the arrays. By 100 ps, $Zn_U^*Zn_C \rightarrow Zn_UZn_C^*$ energy transfer is complete and the features have shifted to the red as expected. The 100 ps spectrum also shows that a small amount of excitation has arrived on the guest to form DPFb*, based on the small Q(0,1) stimulated-emission dip at ~720 nm. By 3.5 ns, DPFb* is essentially fully formed.

TABLE 2: Summary of Rate Constants[a]

rate constant	$(\text{value})^{-1}$
k_1	38 ps
k_2	20−100 ps[b]
k_3	38 ps
k_4	42 ps
M_1	1.1 ns
	0.82 ns[c]
M_2	0.26 ns[c]
M_3	2.6 ns[c]
L_1	≥0.2 ns

[a] See Chart 3 for definition of rate constants. The values were derived from the measured and modeled transient absorption kinetics unless indicated otherwise. [b] We expect that $(k_2)^{-1} \approx 50$ ps but utilize the range 20−100 ps from the kinetic modeling on the compounds studied in ref 40. [c] From Förster calculations in Table 3.

Kinetic profiles (Supporting Information) give time constants of 3.1 ± 0.7 ps, 33 ± 9 ps, and 730 ± 80 ps. The minor, ~3 ps phase can be assigned to $Zn_U^*Zn_U^* \rightarrow Zn_U^*Zn_U$ excited-state annihilation in a small fraction of the arrays in which two zinc porphyrins are excited together. Such a minor component is also observed for ZnZn-*m*/*p* (2.7 ± 0.3 ps) and ZnZn·pyr_2 (3.6 ± 0.8 ps) and in previous studies of arrays containing adjacent zinc porphyrins.[38,47] The ~35 ps component is assigned to energy flow among the zinc porphyrins of the host. This phase is dominated by $k_4 = (42 \text{ ps})^{-1}$ for $Zn_U^*Zn_C \rightarrow Zn_UZn_C^*$ energy transfer since each Zn_U is adjacent to a Zn_C (Chart 3A). On the basis of the arguments given above, we expect that $k_2 \approx (50 \text{ ps})^{-1}$; studies of the arrays studied in the companion paper[40] afford $k_2 = (20-100 \text{ ps})^{-1}$, which we utilized here for the kinetic modeling on Zn_6·DPFb. This modeling also gives an upper limit of $L_1 \leq (200 \text{ ps})^{-1}$.

The 730 ps component is assigned to the lifetime of an excited bookend zinc porphyrin Zn_C^* and is comparable to the value of the 0.9 ns fluorescence component. Thus, the transient absorption data give a yield for energy transfer from host to guest of $\Phi_{trans} = 1 - (0.73/2.1) = 0.65$, which is comparable to the values of 0.63 and 0.57 derived from the fluorescence spectra and lifetimes. Considering the errors in the various measurements, we report $\Phi_{trans} = 0.65$ for Zn_C^*DPFb → Zn_CDPFb* energy transfer. The rate constant for this process is best derived by comparison of the Zn_C^* lifetime (from the transient absorption studies) with that of the reference compounds, which gives $M_1 = [(0.73)^{-1} - (2.1 \text{ ns})^{-1}] = (1.1 \text{ ns})^{-1}$ for Zn_6·DPFb (Chart 3A). The rate constants determined herein are summarized in Table 2.

The distance spanned by the linker between the Zn_C and DPFb porphyrins in the Zn_6·DPFb complex is essentially the same as that within the ZnFb-*p*/*p* dyad, in which the components are covalently joined at their peripheries by a diarylethyne linker with *p*/*p* connectivity (Charts 2B and 4). Energy transfer in the latter has a rate constant of $(24 \text{ ps})^{-1}$ (Chart 5) and is dominated by a TB mechanism, as noted above. The $(1.1 \text{ ns})^{-1}$ rate from a bookend porphyrin of the host to the guest in Zn_6·DPFb is 50-fold smaller, indicating that the electronic coupling for TB transfer via the pyridyl−zinc dative bonding (and coupling of the metal with the porphyrin π-system) is far weaker than when an aryl ring of a linker is attached directly to the porphyrin macrocycle. If the process is exclusively Förster TS in nature, then the efficiency and rate are estimated as $\Phi_{TS} = 0.73$ and $k_{TS} = (0.82 \text{ ns})^{-1}$ (Table 3).[49] This calculated rate constant is

TABLE 3: Förster Energy-Transfer Parameters[a]

donor	acceptor	rate constant	R (Å)	quantum yield	donor lifetime (ns)	$J \times 10^{14}$ (cm^6)	Φ_{TS}	$(k_{TS})^{-1}$ (ns)
Zn_C	DPFb	M_1	17.3	0.037	2.2	4.43	0.73	0.82
Zn_U	DPFb	M_2	14.2	0.034	2.4	5.17	0.90	0.26
Zn_U	DPFb	M_3	20.9	0.034	2.4	5.17	0.48	2.6

[a] Calculations used PhotochemCAD[52] with $\kappa^2 = 0.25$. Distances were derived from those given in ref 19. The fluorescence lifetimes and quantum yields are from Table 1. For donor Zn_C and Zn_U, the fluorescence parameters for ZnU·pyr and ZnU, respectively, were utilized. For acceptor DPFb, an extinction coefficient $\log(\epsilon) = 5.68$ at 423 nm for a toluene solution was used (obtained by solvent replacement of a chloroform solution using the published value[34] $\log(\epsilon) = 5.61$ at 422 nm).

comparable to $M_1 = (1.1\ \text{ns})^{-1}$ obtained above from the lifetime data. The agreement between these values indicates that the host−guest energy-trapping route has a dominant if not exclusive TS character. Visual inspection of the rate constants of the various processes (Chart 3A and Table 2), as well as kinetic modeling of the energy flow, indicates that this pathway (M_1) is the principal route of final energy trapping in Zn_6·DPFb. This is so because the "bookend" Zn_C porphyrins are the lowest-energy chromophores within Zn_6, and rapid TB transfer to these Zn_C units from the Zn_U units competes effectively with TS transfer from Zn_U to the central Fb porphyrin trap, the rate constants of which were estimated from Förster calculations (M_2 and M_3; Chart 3A and Table 3).

IV. Conclusions

The wheel-and-spoke complex Zn_6·DPFb has numerous routes for energy flow within the hexameric host and to the porphyrin guest. The harvested excitation energy flows between adjacent and nonadjacent members of a hexamer and is delivered to the lowest-energy site(s) therein with an effective rate constant of $(\sim 40\ \text{ps})^{-1}$ and with essentially quantitative yield (≥98%). Thus, the subsequent dynamics of energy transfer to the central guest porphyrin dictate the overall rate and yield of energy trapping. The host-to-guest energy-transfer step for Zn_6·DPFb [$M_1 = (1.1\ \text{ns})^{-1}$] occurs from the bookend zinc porphyrins of the host with a yield of 65%. The rate and yield are comparable to those obtained from a Förster calculation, indicating the final phase of energy trapping is predominantly TS in character. Evidently the overall electronic coupling between the host and the guest is too weak to support facile TB energy transfer. The electronic communication is weak because the $p\pi-d\pi$ back-bonding between the zinc and the porphyrin, and the zinc and the pyridyl, are negligible. Accordingly, the electronic characteristics of the guest porphyrin are unperturbed by the presence of the surrounding host. Collectively, these studies elucidate the pathways, mechanisms, rates, and yields for energy transfer in the arrays and self-assembled host−guest complexes. The results form a framework for elucidating the complex energy-flow patterns in arrays described in the following paper, in which one or two Fb porphyrins within the host wheel serve as way stations for energy transfer to the guest. The combined results of these studies provide valuable information for the design of next-generation light-harvesting systems for use in artificial solar-energy conversion systems.

Acknowledgment. This research was supported by grants from the Division of Chemical Sciences, Office of Basic Energy Sciences, Office of Energy Research, U. S. Department of Energy (J.S.L., D.F.B., and D.H.).

Note Added after ASAP Publication. The authorship of the paper has been revised from the version published September 13, 2006; the revised version was published September 20, 2006.

Supporting Information Available: Titration data for the formation of host−guest complexes and time-resolved absorption and kinetic data. This material is available free of charge via the Internet at http://pubs.acs.org.

References and Notes

(1) Imahori, H. *J. Phys. Chem. B* **2004**, *108*, 6130−6143.
(2) Choi, M.-S.; Yamazaki, T.; Yamazaki, I.; Aida, T. *Angew. Chem., Int. Ed.* **2004**, *43*, 150−158.
(3) Sugiura, K.-I. *Top. Curr. Chem.* **2003**, *228*, 65−85.
(4) Kobuke, Y.; Ogawa, K. *Bull. Chem. Soc. Jpn.* **2003**, *76*, 689−708.
(5) Harvey, P. D. In *The Porphyrin Handbook*; Kadish, K. M., Smith, K. M., Guilard, R., Eds.; Academic Press: San Diego, CA, 2003; Vol. 18, pp 63−250.
(6) (a) Kim, D.; Osuka, A. *J. Phys. Chem. A* **2003**, *107*, 8791−8816. (b) Aratani, N.; Osuka, A. *Macromol. Rapid Commun.* **2001**, *22*, 725−740.
(7) (a) Gust, D.; Moore, T. A.; Moore, A. L. *Acc. Chem. Res.* **2001**, *34*, 40−48. (b) Gust, D.; Moore, T. A.; Moore, A. L. *Acc. Chem. Res.* **1993**, *26*, 198−205. (c) Gust, D.; Moore, T. A. *Top. Curr. Chem.* **1991**, *159*, 103−151.
(8) Burrell, A. K.; Officer, D. L.; Plieger, P. G.; Reid, D. C. W. *Chem. Rev.* **2001**, *101*, 2751−2796.
(9) Gribkova, S. E.; Evstigneeva, R. P.; Luzgina, V. N. *Russ. Chem. Rev.* **1993**, *62*, 963−979.
(10) (a) Wasielewski, M. R. *Chem. Rev.* **1992**, *92*, 435−461. (b) Wasielewski, M. R. In *Chlorophylls*; Scheer, H., Ed.; CRC Press: Boca Raton, FL, 1991; pp 269−286.
(11) Boxer, S. G. *Biochim. Biophys. Acta* **1983**, *726*, 265−292.
(12) Satake, A.; Kobuke, Y. *Tetrahedron* **2005**, *61*, 13−41.
(13) Balaban, T. S.; Tamiaki, H.; Holzwarth, A. R. *Top. Curr. Chem.* **2005**, *258*, 1−38.
(14) Drain, C. M.; Bazzan, G.; Milic, T.; Vinodu, M.; Goeltz, J. C. *Isr. J. Chem.* **2005**, *45*, 255−269.
(15) Alessio, E.; Iengo, E.; Marzilli, L. G. *Supramol. Chem.* **2002**, *14*, 103−120.
(16) Chambron, J.-C.; Heitz, V.; Sauvage, J.-P. In *The Porphyrin Handbook*; Kadish, K. M., Smith, K. M., Guilard, R., Eds.; Academic Press: San Diego, CA, 2000; Vol. 6, pp 1−42.
(17) Imamura, T.; Fukushima, K. *Coord. Chem. Rev.* **2000**, *198*, 133−156.
(18) Wojaczynski, J.; Latos-Grazynski, L. *Coord. Chem. Rev.* **2000**, *204*, 113−171.
(19) Li, J.; Ambroise, A.; Yang, S. I.; Diers, J. R.; Seth, J.; Wack, C. R.; Bocian, D. F.; Holten, D.; Lindsey, J. S. *J. Am. Chem. Soc.* **1999**, *121*, 8927−8940.
(20) Yu, L.; Lindsey, J. S. *J. Org. Chem.* **2001**, *66*, 7402−7419.
(21) Tomizaki, K.-y.; Yu, L.; Wei, L.; Bocian, D. F.; Lindsey, J. S. *J. Org. Chem.* **2003**, *68*, 8199−8207.
(22) Van Patten, P. G.; Shreve, A. P.; Lindsey, J. S.; Donohoe, R. J. *J. Phys. Chem. B* **1998**, *102*, 4209−4216.
(23) Sanders, J. K. M. In *The Porphyrin Handbook*; Kadish, K. M., Smith, K. M., Guilard, R., Eds.; Academic Press: San Diego, CA, 2000; Vol. 3, pp 347−368.
(24) Hori, T.; Aratani, N.; Takagi, A.; Matsumoto, T.; Kawai, T.; Yoon, M.-C.; Yoon, Z. S.; Cho, S.; Kim, D.; Osuka, A. *Chem.—Eur. J.* **2006**, *12*, 1319−1327.
(25) Hwang, I.-W.; Yoon, Z. S.; Kim, J.; Kamada, T.; Ahn, T. K.; Aratani, N.; Osuka, A.; Kim, D. *J. Photochem. Photobiol., A* **2006**, *178*, 130−139.
(26) Hajjaj, F.; Yoon, Z. S.; Yoon, M.-C.; Park, J.; Satake, A.; Kim, D.; Kobuke, Y. *J. Am. Chem. Soc.* **2006**, *128*, 4612−4623.
(27) Kuramochi, Y.; Satake, A.; Kobuke, Y. *J. Am. Chem. Soc.* **2004**, *126*, 8668−8669.
(28) Nakamura, Y.; Hwang, I.-W.; Aratani, N.; Ahn, T. K.; Ko, D. M.; Takagi, A.; Kawai, T.; Matsumoto, T.; Kim, D.; Osuka, A. *J. Am. Chem. Soc.* **2005**, *127*, 236−246.
(29) Hwang, I.-W.; Park, M.; Ahn, T. K.; Yoon, Z. S.; Ko, D. M.; Kim, D.; Ito, F.; Ishibashi, Y.; Khan, S. R.; Nagasawa, Y.; Miyasaka, H.; Ikeda, C.; Takahashi, R.; Ogawa, K.; Satake, A.; Kobuke, Y. *Chem.—Eur. J.* **2005**, *11*, 3753−3761.
(30) Kato, A.; Sugiura, K.-I.; Miyasaka, H.; Tanaka, H.; Kawai, T.; Sugimoto, M.; Yamashita, M. *Chem. Lett.* **2004**, *33*, 578−579.
(31) (a) Mongin, O.; Schuwey, A.; Vallot, M.-A.; Gossauer, A. *Tetrahedron Lett.* **1999**, *40*, 8347−8350. (b) Rucareanu, S.; Mongin, O.;

Schuwey, A.; Hoyler, N.; Gossauer, A.; Amrein, W.; Hediger, H.-U. *J. Org. Chem.* **2001**, *66*, 4973−4988. (c) Rucareanu, S.; Schuwey, A.; Gossauer, A. *J. Am. Chem. Soc.* **2006**, *128*, 3396−3413.

(32) (a) Anderson, H. L.; Hunter, C. A.; Sanders, J. K. M. *J. Chem. Soc., Chem. Commun.* **1989**, 226−227. (b) Anderson, S.; Anderson, H. L.; Sanders, J. K. M. *Angew. Chem., Int. Ed. Engl.* **1992**, *31*, 907−910. (c) Anderson, S.; Anderson, H. L.; Bashall, A.; McPartlin, M.; Sanders, J. K. M. *Angew. Chem. Int. Ed. Engl.* **1995**, *34*, 1096−1099. (d) McCallien, D. W. J.; Sanders, J. K. M. *J. Am. Chem. Soc.* **1995**, *117*, 6611−6612. (e) Anderson, H. L.; Anderson, S.; Sanders, J. K. M. *J. Chem. Soc., Perkin Trans. 1* **1995**, 2231−2245.

(33) Slone, R. V.; Hupp, J. T. *Inorg. Chem.* **1997**, *36*, 5422−5423.

(34) Ambroise, A.; Li, J.; Yu, L.; Lindsey, J. S. *Org. Lett.* **2000**, *2*, 2563−2566.

(35) (a) Moore, J. S. *Acc. Chem. Res.* **1997**, *30*, 402−413. (b) Grave, C.; Schlüter, A. D. *Eur. J. Org. Chem.* **2002**, 3075−3098. (c) Höger, S. *J. Polym. Sci., Part A: Polym. Chem.* **1999**, *37*, 2685−2698.

(36) Tiede, D. M.; Zhang, R.; Chen, L. X.; Yu, L.; Lindsey, J. S. *J. Am. Chem. Soc.* **2004**, *126*, 14054−14062.

(37) Holten, D.; Bocian, D. F.; Lindsey, J. S. *Acc. Chem. Res.* **2002**, *35*, 57−69.

(38) Hindin, E.; Forties, R. A.; Loewe, R. S.; Ambroise, A.; Kirmaier, C.; Bocian, D. F.; Lindsey, J. S.; Holten, D.; Knox, R. S. *J. Phys. Chem. B* **2004**, *108*, 12821−12832.

(39) Lammi, R. K.; Ambroise, A.; Balasubramanian, T.; Wagner, R. W.; Bocian, D. F.; Holten, D.; Lindsey, J. S. *J. Am. Chem. Soc.* **2000**, *122*, 7579−7591.

(40) Song, H.; Kirmaier, C.; Schwartz, J. K.; Hindin, E.; Yu, L.; Bocian, D. F.; Lindsey, J. S.; Holten, D. *J. Phys. Chem. B* **2006**, *110*, 19131−19139.

(41) Hsiao, J.-S.; Krueger, B. P.; Wagner, R. W.; Johnson, T. E.; Delaney, J. K.; Mauzerall, D. C.; Fleming, G. R.; Lindsey, J. S.; Bocian, D. F.; Donohoe, R. J. *J. Am. Chem. Soc.* **1996**, *118*, 11181−11193.

(42) Seybold, P. G.; Gouterman, M. *J. Mol. Spectrosc.* **1969**, *31*, 1−13.

(43) Kee, H. L.; Kirmaier, C.; Yu, L.; Thamyongkit, P.; Youngblood, W. J.; Calder, M. E.; Ramos, L.; Noll, B. C.; Bocian, D. F.; Scheidt, W. R.; Birge, R. R.; Lindsey, J. S.; Holten, D. *J. Phys. Chem. B* **2005**, *43*, 20433−20443.

(44) Kee, H. L.; Laible, P. D.; Bautista, J. A.; Hanson, D. K.; Holten, D.; Kirmaier, C. *Biochemistry* **2006**, *45*, 7314−7322.

(45) Yang, S. I.; Lammi, R. K.; Prathapan, S.; Miller, M. A.; Seth, J.; Diers, J. R.; Bocian, D. F.; Lindsey, J. S.; Holten, D. *J. Mater. Chem.* **2001**, *11*, 2420−2430.

(46) Barshop, B. A.; Wrenn, R. F.; Frieden, C. *Anal. Biochem.* **1983**, *130*, 134−145.

(47) del Rosario Benites, M.; Johnson, T. E.; Weghorn, S.; Yu, L.; Rao, P. D.; Diers, J. R.; Yang, S. I.; Kirmaier, C.; Bocian, D. F.; Holten, D.; Lindsey, J. S. *J. Mater. Chem.* **2002**, *12*, 65−80.

(48) For Zn_6·pyr_3, the time constant varies from ∼30 to ∼50 ps with probe wavelength. This variation most likely arises because statistically there will be a fraction of the arrays in which a photoexcited uncoordinated zinc porphyrin will have two adjacent coordinated zinc porphyrins (which by itself would give one-half the Zn_U^* lifetime) as well as a nonadjacent uncoordinated zinc porphyrin to which it can transfer energy via a superexchange mechanism with a rate ∼10-fold less than transfer to an adjacent chromophore.

(49) In the Förster calculations (Table 3), a value of $\kappa^2 = 0.25$ has been used. This value is appropriate for energy transfer from a bookend porphyrin to the guest porphyrin assuming (1) free rotation of the guest relative to the host during the lifetime of the donor excited state (dynamically averaged limit) and (2) the transition-dipole direction in the guest porphyrin lies along the N−N axis.

(50) Yang, S. I.; Seth, J.; Strachan, J.-P.; Gentemann, S.; Kim, D.; Holten, D.; Lindsey, J. S.; Bocian, D. F. *J. Porphyrins Phthalocyanines* **1999**, *3*, 117−147.

(51) Tomizaki, K.-Y.; Loewe, R. S.; Kirmaier, C.; Schwartz, J. K.; Retsek, J. L.; Bocian, D. F.; Holten, D.; Lindsey, J. S. *J. Org. Chem.* **2002**, *67*, 6519−6534.

(52) Dixon, J. M.; Taniguchi, M.; Lindsey, J. S. *Photochem. Photobiol.* **2005**, *81*, 212−213.